A Biosensor for Inorganic Phosphate Using a Rhodamine-Labeled Phosphate Binding Protein †

ARTICLE *in* BIOCHEMISTRY · JANUARY 2007

Impact Factor: 3.02 · DOI: 10.1021/bi060960j · Source: PubMed

4 AUTHORS, INCLUDING:

Michael P Okoh
University of Abuja
16 PUBLICATIONS **132** CITATIONS
SEE PROFILE

Martin R. Webb
The Francis Crick Institute
153 PUBLICATIONS **4,629** CITATIONS
SEE PROFILE

A Biosensor for Inorganic Phosphate Using a Rhodamine-Labeled Phosphate Binding Protein†

Michael P. Okoh, Jackie L. Hunter, John E. T. Corrie, and Martin R. Webb*

MRC National Institute for Medical Research, Mill Hill, London NW7 1AA, United Kingdom

Received May 15, 2006; Revised Manuscript Received October 3, 2006

ABSTRACT: A novel biosensor for inorganic phosphate (P_i) has been developed based on the phosphate binding protein of *Escherichia coli*. Two cysteine mutations were introduced and labeled with 6-iodoacetamidotetramethylrhodamine. When physically close to each other and correctly oriented, two rhodamine dyes interact to form a noncovalent dimer. In this state, they have little or no fluorescence, unlike the high fluorescence intensity of monomeric rhodamine. The labeling sites were so placed that the distance and orientation between the rhodamines change as a consequence of the conformational change associated with P_i binding. This movement alters the extent of interaction between the dyes. The best mutant of those tested (A17C, A197C) gives rise on average to ∼18-fold increase in fluorescence intensity as P_i binds. The kinetics of interaction with P_i were measured at 10 °C. Under these conditions, the fluorescence increase associated with P_i binding has a maximum rate of 267 s^{-1}. The P_i dissociation rate is 6.6 s^{-1}, and the dissociation constant is 70 nM. An application of the sensor is demonstrated for measuring ATP hydrolysis in real time as a helicase moves along DNA. Advantages of the new sensor are discussed, both in terms of the use of a rhodamine fluorophore and the potential of this double labeling strategy.

INTRODUCTION

Inorganic phosphate (P_i) is a product of many enzymic reactions. For example, there are a wide variety of nucleoside triphosphatases involved in a multitude of cellular processes. Protein phosphatases are also widespread, including those involved in control of the phosphorylation state of many proteins. Thus, measurement of P_i is an important target for understanding cellular activities involving such proteins. As many phosphatases, GTPases, and ATPases are involved in control of cellular events, this measurement is also potentially important for determining effects of drug action on pathways within cells.

A varied range of assays for P_i has been described (summarized in ref *1*). Of particular relevance to this current work, we previously developed a fluorescent biosensor based on the phosphate binding protein (PBP)[1] from *Escherichia coli* (*2*). This protein is the primary phosphate receptor of the ABC transport system and belongs to a class of bacterial proteins that scavenge for specific, essential small molecules in the periplasm prior to their import through the cell membrane. Examples of such types of molecules are inorganic ions, sugars, and amino acids. Generally these periplasmic proteins are robust to denaturation and bind their target molecule very specifically and tightly. These properties are potentially advantageous for use in biosensors, and several of these proteins, apart from the phosphate binding protein, have been targets for development in this way (*3*−*8*).

The phosphate binding protein (PBP) has two domains, hinged so they close around the phosphate that binds in the cleft between them (*9*). This conformation change provided one mechanism for development of the previous sensor. A single coumarin fluorophore labeled a cysteine that was introduced by mutation on the surface of the protein at the edge of the phosphate-binding cleft. The environmental change to the fluorophore on cleft closure gives rise to an order of magnitude increase in fluorescence. The detailed mechanism and structural basis for this have been described (*10*, *11*). In related work, the fluorescence changes for the maltose binding protein, labeled at three different sites, have also been correlated with cleft closure (*12*). Separately, cleft closure has also been demonstrated in the maltose binding protein by attaching identical spin labels to each domain. EPR spectral changes upon binding maltose or related sugars were used to differentiate modes of binding, of which only cleft closure led to sugar transport (*13*).

The phosphate binding protein is very specific for inorganic phosphate and binds phosphate esters and anhydrides very weakly. This protein labeled with the coumarin, as described above (MDCC-PBP), has proved useful as a biosensor to measure rapid phosphate release from a wide variety of ATPases and GTPases. These range from stopped-flow measurements, where release of ∼1 μM Pi or less

† This work was supported by the Medical Research Council, U.K. and in part by an EU Research Training Network (HRPN-CT-2000-00091). Part of this work is subject of a U.K. patent application (0517855.3).

* Corresponding author. Tel: (+44) 20 8816 2078. Fax: (+44) 20 8906 4477. E-mail: mwebb@nimr.mrc.ac.uk.

[1] Abbreviations: PBP, phosphate binding protein; MDCC, *N*-[2-(1-maleimidyl)ethyl]-7-diethylaminocoumarin-3-carboxamide; MDCC-PBP, A197C mutant of PBP labeled with MDCC; PNPase, purine nucleoside phosphorylase; DTNB, 5,5′-dithio-bis(2-nitrobenzoic acid); 6-IATR, 6-iodoacetamidotetramethylrhodamine; 5-IATR, 5-iodoacetamidotetramethylrhodamine; RRC2M, rhodamine red C2 maleimide; rhodamine-PBP, A17C-A197C double mutation PBP in which each cysteine is labeled with 6-IATR; BSA, bovine serum albumin.

10.1021/bi060960j CCC: $33.50
Published on Web 11/15/2006

occurs (*14*−*17*), to measurements of several hundred micromolar P_i in single muscle fibers (*18*).

Here we describe a development of a biosensor for P_i using the same protein but an alternative strategy for labeling, with the aim of widening the range of applications and providing a number of advantages over the previous biosensor. We make use of the fact that some fluorophores can stack, either with themselves or another aromatic molecule to form a noncovalent complex with different optical properties from those of the monomeric dye. Molecular stacking takes place through the physical interaction of ground states of the two moieties, whereas fluorescence quenching occurs through a phenomenon called exciton coupling (*19*). Stacking can occur between identical or different chromophores. Although the magnitude of the band splitting that occurs in molecular excitons has an inverse r^3 dependence (*19*−*21*), this does not directly address the question of the propagation distance for the effect, because its operation presumably depends upon the ground-state stacking of the two monomers. This would require physical interaction, and the relative orientation is also likely to be important for optimal fluorescence quenching.

We confine ourselves here to labeling with rhodamines, as two identical rhodamines can stack with each other if in close proximity. Free rhodamine has high fluorescence and good wavelengths for excitation and emission. A single type of label avoids the problem of introducing two different labels specifically onto a single polypeptide chain. Rhodamines can stack to form these noncovalent dimers at high concentrations in solution (*22*, *23*) or when constrained close together (*24*−*26*). The dimer ($\lambda_{max} \sim 520$ nm) has a different absorbance spectrum from the monomer ($\lambda_{max} \sim 550$ nm) and has little or no fluorescence in comparison with the monomer (*27*). If two rhodamines are present on the same molecule or molecular complex and within interaction distance, intramolecular rhodamine stacking is likely to be independent of concentration.

This property of rhodamines has been used previously in a number of assays. For example, two rhodamines at the N- and C-termini of a peptide can be separated by protease cleavage, giving rise to monomer formation and a large increase in fluorescence (*24*−*26*). If the 5′- and 3′-ends of complementary oligonucleotides are labeled with rhodamine, these can dimerize on duplex formation: this can be used as an assay for duplex formation and unwinding (*28*). Similarly, a hairpin oligonucleotide structure, labeled at each end with a rhodamine, provides a molecular beacon to assay for a complementary strand (*29*). The proportion of rhodamine dimer has been used as evidence for a conformation change on binding ribosomal proteins to the ribosome (*30*).

Here we show that two rhodamines attached to a single monomeric protein can respond to a conformation change by a change in the stacking interaction. This, in turn, results in a large fluorescence change in response to the P_i-driven conformation change. We describe the use of this labeled protein as a phosphate biosensor that has advantages over the single coumarin-labeled protein, in part because of the advantageous fluorescence properties of rhodamines. However, there are also advantages because the basis of the fluorescence change is due to interaction of the two labels with each other, rather than interaction of one label with the binding cleft.

P_i contamination is ubiquitous at low but significant levels, particularly in biological preparations, but also in buffers and on surfaces of glass, etc. The PBP readily binds this contaminant P_i so that some or all of its binding capacity and ability to measure newly generated P_i may be lost. An essential part of applying this biosensor is the use of a phosphate mop (*2*, *31*). This enzymic procedure uses purine nucleoside phosphorylase to sequester such contaminant P_i as ribose 1-phosphate that does not bind significantly to the phosphate binding protein. The use of this phosphate mop enables the biosensor to be obtained essentially free of P_i.

EXPERIMENTAL PROCEDURES

"Bacterial" PNPase was from Sigma. The lyophilized powder was dissolved in water to 1000 unit mL^{-1} and stored in aliquots at −80 °C. The DNA helicase PcrA was prepared as described (*32*). The oligonucleotide dT_{20} was from Genosys. Other proteins, substrates, and cofactors were from Sigma. 6-Iodoacetamidotetramethylrhodamine (6-IATR) and 5-IATR were synthesized as described (*33*, *34*). RRC2M was from Molecular Probes, OR.

Preparation of Mutant PBP. Mutants of phosphate binding protein were prepared in plasmid PSN5182 using the Quikchange site-directed mutagenesis kit (Stratagene) and then amplified by polymerase chain reaction (PCR). The products were transformed into the *Escherichia coli* strain DH5α (library efficiency, Invitrogen). The plasmid was purified using Qiaprep kit (Qiagen) and analyzed by 1% agarose gel electrophoresis. DNA sequencing (MWG-Biotech) of the plasmid DNA confirmed the desired changes in all cases. The DNA was transformed into *E. coli* strain ANCC75 for protein expression.

Growth conditions and protein purification were essentially as described for the A197C mutant PBP (*10*), except that dithiothreitol (1 mM) was added to all solutions from the osmotic shock through to the stock storage buffer. The protein was stored at −80 °C in aliquots at ∼1 mM concentration. A 4 L culture gave ∼75 mg of purified protein with >95% purity.

Labeling Mutant PBPs. The exact time and conditions for labeling cysteine mutants depended both on the reactivity of the label and the solvent accessibility of the thiol. Conditions are given here for the labeling of the double mutant, A17C-A197C. Prior to labeling, fresh dithiothreitol to a final concentration of 10 mM was added to the protein at ∼1 mM, which was then desalted by gel filtration on a PD10 column (Amersham) in 10 mM Tris•HCl pH 8.0, degassed by bubbling nitrogen through the solution.

The protein was labeled on a scale of 40 mg. The following solution was incubated for 15 min at 20 °C under nitrogen in 50 mM Tris•HCl pH 8.1 to remove P_i: 100 μM mutant PBP, 200 μM 7-methylguanosine, 0.2 unit mL^{-1} PNPase. The protein was then labeled by adding 800 μM 6-IATR (from a stock solution of ∼20 mM in dimethylformamide). The solution was mixed end-over-end with protection from light at 22 °C for 2 h. The solution was made 1.6 mM in sodium 2-mercaptoethanesulfonate, incubated for 20 min and filtered through a 0.2 μm polysulfone membrane. Rhodamine that was not bound to the protein was removed by gel filtration on a 100 mL P4 column (Bio-Rad), equilibrated in 10 mM Tris•HCl pH 8.0 at room temperature. The labeled

protein was then purified by ion exchange chromatography at 4 °C on a 20 mL column of Q Sepharose FF (Amersham), equilibrated in 10 mM Tris•HCl pH 8.0 at 4 °C, using a 400 mL gradient from 0 to 200 mM NaCl in 10 mM Tris•HCl pH 8.0.

After concentration by ultrafiltration through a YM10 membrane (Amicon), the labeled protein was purified further at room temperature on a MonoQ HR 10/10 column (Amersham), equilibrated in 10 mM Tris•HCl pH 8.5, 15 mM KCl. Protein was eluted at 2.5 mL min^{-1} with a 150 mL gradient from 15 to 30 mM NaCl in 10 mM Tris•HCl pH 8.5. The peak corresponding to doubly labeled protein was concentrated as above, diluted with several volumes of 10 mM Tris•HCl pH 8.0, reconcentrated, and then stored at −80 °C in aliquots at ∼1 mM. The concentration of the rhodamine-PBP was calculated using an extinction coefficient of 108 mM^{-1} cm^{-1} at 526 nm, determined as described in Results.

The molecular masses of unlabeled and labeled proteins were determined by electrospray mass spectrometry as described previously (*10*). The reactivity of thiols of unlabeled protein was determined by reaction with DTNB as described previously (*10*), except that the solution conditions were 1 mM DTNB, 27 μM PBP in 100 mM Tris•HCl (pH 8.0) either with 270 μM P_i or with 300 μM 7-methylguanosine and 1 unit mL^{-1} purine nucleoside phosphorylase. The latter pair of reagents acts as a phosphate mop to remove contaminant P_i, as described in the Introduction

Absorbance and Fluorescence Measurements. Absorbance spectra were obtained on a Beckman DU640 spectrophotometer. Fluorescence measurements were obtained on a Cary Eclipse fluorimeter with xenon lamp. Stopped-flow experiments were carried out on a HiTech SF61MX apparatus, with a mercury-xenon lamp and HiTech IS-2 software. There was a monochromator and 4-mm slits on the excitation light (550 nm) and a 570 nm cutoff filter on the emission. The stated concentrations are those in the mixing chamber, unless shown otherwise. Data were fitted to theoretical curves using either the HiTech software or Grafit (*35*).

RESULTS

Developing the Biosensor. To implement the labeling strategy, it was necessary to introduce two thiols into PBP that could be readily labeled with rhodamines, and this was most likely to be achieved with cysteines that are exposed at the surface. Furthermore, the cysteines must be sufficiently close for the rhodamines to interact with each other. The distance between them must change between the phosphate-bound and the phosphate-free structures to enable there to be a possibility of a change in extent of interaction. Wild-type PBP has no cysteines, and crystal structures were examined to plan the location of two introduced cysteines. We used our own structure of MDCC-PBP with P_i bound (*11*). In addition, a mutant PBP with reduced affinity for P_i has been described, enabling a high-resolution structure to be obtained of the P_i-free form (*36*). Examination of these structures identified several pairs of amino acids on the surface that were not apparently involved in side-chain interactions and had their α-carbons ∼1 nm apart. The amino acids were generally within regions of secondary structure such as α-helix, so that there might be local rigidity. In addition, the distance between these pairs was different in the apo and P_i-bound structures.

Table 1: Summary of Cysteine Mutants Surveyed: Change in α-Carbon Distances between the Cysteines and the Fluorescence Changes for the Proteins, Doubly Labeled with 6-IATR

	distances between cysteine α-carbons[a]		
mutations	-P_i (nm)	+P_i (nm)	fluorescence ratio[b]
A17C, A197C	1.6	1.3	18
N226C, S299C	1.1	1.6	7
E247C, S299C	1.6	2.2	4
E222C, S299C	1.5	1.8	1[c]
K229C, E302C	1.2	1.7	10

[a] Distances were obtained from crystal structures of P_i-saturated (pdb 1a54, *11*) and P_i-free (pdb 1oib, *36*) PBP. [b] The fluorescence changes are from a survey without complete optimization of the labeling or purification for each mutant. The ratio of fluorescence is that of saturating P_i to that with the phosphate mop, as described in the text. [c] This labeled protein did not purify well, resulting in ∼10% singly labeled material with a large contribution to background fluorescence.

Two different regions of the protein were examined. First, as the cleft between the domains closes on P_i binding, the two surface regions on either side of this cleft get closer to each other. However, the surface movement is complex as the cleft closure is produced not only by hinge bending but also by a twisting of the domains relative to each other. This movement is also transmitted to structural changes in other parts of the protein. The hinge is formed by two extended pieces of the polypeptide, located somewhat centrally in the protein. So when the P_i-binding cleft closes on one side of the hinge, there is in essence a rocking motion of the domains relative to each other and a new, small "cleft" forms on the opposite face of the protein. Here, we chose pairs of amino acids that moved apart on P_i binding.

Several pairs of mutation sites were identified, mainly on the opposite face from the binding cleft that fulfilled the requirements outlined above. Four such pairs were tested: K229C-E302C, E247C-S299C, E222C-S299C, and N226C-S299C. In addition, the A17C-A197C mutant might monitor the movement at the binding cleft, because the two mutated residues are on opposite sides of this cleft. The distances between α-carbons of the cysteine pairs in the presence and absence of P_i are listed in Table 1.

Three thiol-selective rhodamines were used in labeling tests: two iodoacetamides, 6-IATR and 5-IATR, and one maleimide, RRC2M. It became apparent that the signal response is very dependent not only the position of the rhodamines but also on the degree of purity of the final, doubly labeled product. The latter depends on the ease of labeling, as singly or triply labeled protein has an unpaired rhodamine and so results in high fluorescence (see below). The degree of purity also depends on the resolution obtained during the purification.

All five PBPs with double cysteine mutations were tested with 6-IATR, and the outcome of this survey is in Table 1. The two best were the K229C-E302C (10-fold fluorescence increase with P_i) and A17C-A197C proteins (18-fold increase) and these were evaluated further. Two other fluorophores were tested with the best mutant, A17C-A197C. The RRC2M did not label well and gave a product with little fluorescence change. 5-IATR labeled the two cysteines of

this mutant, but the product gave only ~2.5-fold increase. The best combination that was identified from this survey is the double mutant, A17C-A197C labeled with 6-IATR. This was used for the main study and is referred to below as rhodamine-PBP.

To optimize labeling conditions, the reactivity of the two thiols of this A17C-A197C mutant with DTNB was investigated using the two single cysteine proteins in addition to the double cysteine mutant itself. The kinetics of this reaction with A197C have been reported previously (*10*): its reactivity is greatly inhibited by P_i binding. Using similar conditions here, the reaction rate constants under pseudo-first-order conditions at 21 °C were as follows: A197C ($+P_i$) 0.04 min^{-1}, ($-P_i$) 4.1 min^{-1}, A17C ($+P_i$) 1.1 min^{-1}, ($-P_i$) 1.0 min^{-1}, A197C-A17C ($+P_i$) biphasic 0.9 min^{-1} and 0.01 min^{-1}, ($-P_i$) 1.1 min^{-1}. In the final case, it was not possible to distinguish two phases satisfactorily with the manual mixing protocol used.

Labeling outcomes can occur other than attachment of a rhodamine to each of the two cysteines. In trial labeling, it was possible to incorporate a third rhodamine very slowly, presumably by derivatization of a lysine. Similar lysine labeling had been observed in preparations of MDCC-PBP when nonoptimized labeling conditions were used (*10*). Incomplete labeling of the two thiols is also possible. Either of these unwanted labeling patterns would give rise to a protein-attached rhodamine that has no partner with which to stack and would have high fluorescence, probably similar to free rhodamine in solution. This non-stacked rhodamine is not likely to respond to P_i binding and so would contribute significant background fluorescence intensity. The different labeled species (one, two, or three rhodamines per protein molecule) were identified through a combination of chromatography and mass spectrometry and indicated that this is the case. It was therefore important to obtain the doubly labeled molecule as pure as possible, and this was achieved by a 2-fold strategy. First, the labeling conditions were optimized. Second, the purification of the labeled protein was developed to separate the different labeled species and obtain a homogeneous product, at least as shown by electrospray mass spectrometry.

Fluorescence and Absorbance Properties of Rhodamine-PBP. The final conditions, by which A17C-A197C PBP was labeled with 6-IATR and purified, are given in Experimental Procedures. The fluorescence of this resulting rhodamine-PBP is much lower than that expected for two independent monomers, presumably because the two rhodamines can interact via stacking. The absorbance spectrum of this purified rhodamine-PBP shows a change on binding P_i with the peak at 554 nm increasing ~2.5-fold on saturation with P_i (Figure 1). There is a concomitant decrease in the peak at 515 nm. The fluorescence spectra also show a large change on binding P_i (Figure 2). At 578 nm (emission λ_{max}), the increase is up to 30-fold. The amplitude of the increase depends on the resolution of different labeled species by the final ion exchange column and is typically ~18-fold. The fluorescence changes at pH 6.5 and 8.0 are similar to that at pH 7.0. The fluorescence excitation spectrum has a maximum that coincides with the absorbance peak at 554 nm. There is much less fluorescence excitation at the position of the second absorbance peak at 515 nm.

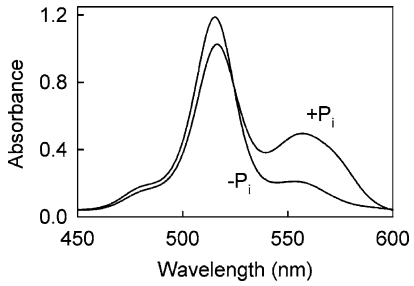

FIGURE 1: Absorbance spectra of rhodamine-PBP. The spectra were run in 10 mM PIPES pH 7.0 buffer with 6.2 μM protein and either 10 μM P_i ($+P_i$) or phosphate mop (4 unit mL^{-1} PNPase, 250 μM 7-methylguanosine) ($-P_i$).

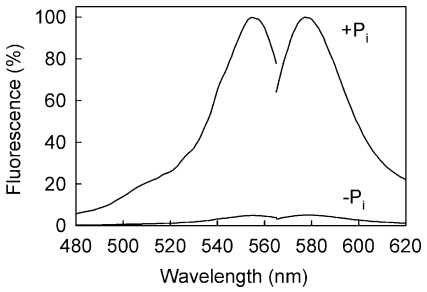

FIGURE 2: Fluorescence excitation and emission spectra of rhodamine-PBP. Conditions are as in Figure 1, except that PNPase was added to 8 unit mL^{-1} and 7-methylguanosine to 333 μM. Excitation was at 555 nm for the emission spectrum. Emission was measured at 575 nm for the excitation spectrum.

The fluorescence of the doubly labeled PBP contrasts with that of the proteins with only one cysteine labeled. This was investigated by labeling the two single mutant proteins, A17C and A197C. In each case, the rhodamine fluorescence was much higher than the doubly labeled protein in the absence of P_i and was only slightly affected by addition of P_i. Similarly, the absorbance peak at ~550 nm was much larger than that at ~520 nm. In the case of labeled A17C, the absorbance at 555 nm decreased by ~6% and the fluorescence decreased by 25% on saturation with P_i. Labeled A197C showed a 14% increase both in absorbance at 555 nm and in fluorescence on saturation with P_i.

It became apparent from two results that the published extinction coefficient for a small molecule thiol adduct of 6-IATR (52000 M^{-1} cm^{-1} at its isosbestic point of 528 nm) (*33*) is not applicable to rhodamine-PBP. First, when this extinction coefficient was used to calculate protein concentration, the apparent binding capacity from P_i titrations (see below) was greater than 100%. Second, the isosbestic point in the absorbance spectrum of rhodamine-PBP, determined using different concentrations of P_i, was found to be 526 nm. Thus, an extinction coefficient of 108 mM^{-1} cm^{-1} at 526 nm was calculated for the doubly labeled protein, assuming 100% binding capacity for P_i in such titrations. The value is based on an average of six titrations. The concentrations of other rhodamine-PBP samples were then calculated from this extinction coefficient.

A titration of the doubly labeled protein with P_i shows that the fluorescence increases linearly over most of its range (Figure 3). As described in Experimental Procedures, the binding capacity is assumed to be ~100%, after taking into account the small amount of P_i present initially through contamination. This high stoichiometry is in contrast to MDCC-PBP, where a similar titration typically shows ~70%

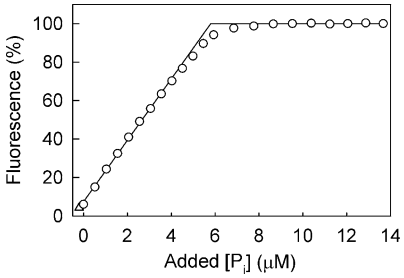

FIGURE 3: Titration of P_i into rhodamine-PBP. Aliquots of P_i were added to 6.1 μM rhodamine-PBP, and the fluorescence was measured at 575 nm, exciting at 555 nm (circles). The data are normalized to 100% for the fluorescence at high [P_i]. The triangle represents the fluorescence after a similar rhodamine-PBP solution was treated with phosphate mop (2.5 unit mL^{-1} PNPase, 200 μM 7-methylguanosine) for 15 min, giving PBP that is approximately P_i-free. The lines are a best fit to data from 0 to 4.5 μM added P_i, and a horizontal line fitting data from 7.5 μM. The intercept of these two lines is a measure of the capacity of the rhodamine-PBP for P_i, once the slight amount of P_i prebound to the protein is taken into account (*1*).

capacity and a more curved titration: possible reasons for this difference are discussed later. This titration was done at a protein concentration that was too high to get an accurate value for the dissociation constant, but a value for this was obtained from kinetic data as described below.

The Doubly Labeled K229C-E302C Protein. This has a similar set of absorbance and fluorescence results, albeit with a lower fluorescence enhancement, and the fluorescence titration with P_i indicated that the protein is ~100% active (data not shown). These distinct changes in the absorbance spectrum suggest the basis of the main fluorescence change for this mutant is also the change in rhodamine stacking.

Affinity of Other Anions for Rhodamine-PBP. Several analogues of P_i, as well as pyrophosphate and purine nucleotides were tested with A17C-A197C rhodamine-PBP by measuring any fluorescence response (Table 2). Among the analogues, only arsenate showed a large fluorescence increase when added to the sensor. A titration indicated that this analogue bound to PBP with a dissociation constant of 1.9 μM. Although the arsenate and phosphate anions are similar in size and shape, there are several crystallographic examples of bonds to As being slightly longer than bonds to P, with an example being a 10% difference for an arsenate and phosphate (*37*). Other studies show substantial kinetic differences between hydrolysis of phosphates and arsenates: see Byers et al. (*38*) and Ali and Dixon (*39*) for examples and references to earlier work. The fact that all four oxygens of P_i are involved in hydrogen bonds within the binding site (*9*) means even small changes to the ligand may result in a less optimal binding.

Pyrophosphate gave very little response, but results with nucleotides were variable, probably because of contamination by P_i. It is likely that the phosphate mop is not effective in the presence of high concentrations of the nucleotides due to inhibition of PNPase. It is therefore probable that most of the fluorescence increase with the nucleotides is due to remnant P_i contamination and that the nucleotides bind only weakly. These results are consistent with the high specificity seen previously with wild-type and MDCC-labeled PBP (*2*, *9*).

Kinetics of P_i Binding and Dissociation. We have determined the association and dissociation kinetics of P_i and rhodamine-PBP. The association kinetics were determined by rapidly mixing P_i with the protein in a stopped-flow apparatus (Figure 4). By repeating the measurement at increasing P_i concentrations, it is apparent that the rate reaches a limiting high value. The data are fit by single exponentials whose rates saturate at high P_i concentrations. They are, therefore, most simply interpreted in terms of a two-step mechanism, shown in eq 1, with rapid binding (step 1) then a conformation change (step 2) that includes the cleft closure:

$$\mathrm{PBP} + \mathrm{P_i} \overset{1}{\rightleftharpoons} \mathrm{PBP{\cdot}P_i} \overset{2}{\rightleftharpoons} \mathrm{PBP^*{\cdot}P_i} \qquad (1)$$

The model assumes that the fluorescence change is solely on step 2 and is likely to be concomitant with the cleft closure. It is this process that limits the overall rate at high P_i concentration. The data in Figure 4 were fitted to a hyperbola to give $1/K_1 = 2.2$ μM and $k_{+2} + k_{-2} = 267$ s^{-1}.

To measure the dissociation kinetics, a preformed complex of P_i with rhodamine-PBP was mixed with a large excess of wild-type PBP (Figure 4C). For these conditions, the fluorescence kinetics reflect the dissociation rate constant (k_{-2}) at 6.6 s^{-1}, as a calculation from previous data (*2*, *10*) shows that binding to wild-type PBP is fast. The overall dissociation constant is given by $k_{-2}/k_{+2}K_1$ and is 70 nM.

A Real-Time Assay of ATP Hydrolysis by a DNA Helicase. A test reaction was performed to demonstrate that rhodamine-PBP could successfully monitor P_i in real time (Figure 5). DNA helicases such as PcrA hydrolyze ATP to drive translocation along DNA. Starting with a complex in which PcrA is bound to an oligonucleotide, mixing with ATP causes the protein to move in an ATP-dependent reaction to the 5′-end. After that, slow dissociation and rebinding lead to slower steady-state ATP hydrolysis. These phases were characterized previously (*40*). The data presented here are

Table 2: Fluorescence Changes with Phosphate Analogues, Pyrophosphate, and Nucleotides When Added to Rhodamine-PBP[a]

species	increase in fluorescence (%)[b]
1 mM ammonium sulfate	0
100 μM sodium arsenate[c]	713
100 μM sodium vanadate	40
100 μM beryllium chloride + 100 mM sodium fluoride	3
100 μM aluminum chloride + 100 mM sodium fluoride	3
100 μM sodium pyrophosphate[d]	5
100 μM ATP[d]	167
100 μM ADP[d]	82
100 μM GDP[d]	219

[a] The various species were added at the concentrations shown to a solution containing 5 μM rhodamine-PBP in 20 mM PIPES pH 7.0. Fluorescence was measured as in Figure 2. Subsequent addition of saturating P_i gave a similar fluorescence enhancement to that produced by P_i in the absence of the competitor [b] The fluorescence increase is the ratio of the change in fluorescence to the baseline fluorescence in the absence of additions, expressed as a percentage. [c] A titration curve for arsenate was obtained as described in Figure 3, except that 0.2 μM rhodamine-PBP was used and 5 μM BSA was present to inhibit surface adsorption. The data were fit to a hyperbola to give a dissociation constant of 1.9 μM. [d] These were treated with phosphate mop for 10 min prior to addition: the following were incubated for 10 min at room temperature in the PIPES buffer: 6.1 mM nucleotide or pyrophosphate, 200 μM 7-methylguanosine, 0.1 unit mL^{-1} PNPase.

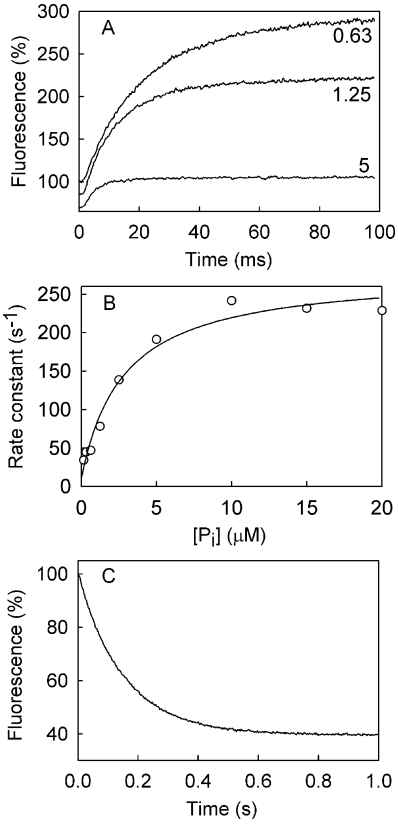

FIGURE 4: Kinetics of P_i association with and dissociation from rhodamine-PBP. (A) In the stopped-flow apparatus, rhodamine-PBP (0.2 μM) was mixed with P_i at the concentrations shown at 10 °C in 10 mM PIPES, pH 7.0. A representative set of fluorescence traces is shown and the labels are the micromolar P_i concentrations. Each trace is normalized to 100% for the initial intensity but offset by 15% from each other. Note that as the concentration of P_i and the rate increase, a significant proportion of the time course is lost in the dead time of the stopped-flow instrument. This causes the apparent decrease in intensity. (B) The data were fitted to a hyperbola as described in the text: Observed rate constant = $k_{+2}/(1 + K_1/[P_i]) + k_{-2}$. Each point represents an average of three measurements. (C) Dissociation kinetics were measured by mixing 0.25 μM rhodamine-PBP containing 0.06 μM P_i with a large excess (10 μM) wild-type PBP using the same solution conditions as in A. BSA (2.5 μM) was present with rhodamine-PBP to minimize any adsorption to surfaces. PNPase (0.25 unit mL^{-1}) and 100 μM 7-methylguanosine were present with the wild-type PBP to ensure that it was free of P_i prior to mixing. The kinetics of the fluorescence change are limited by the P_i dissociation rate, as shown by varying the concentration of wild-type PBP. A best fit exponential gave a rate of 6.6 s^{-1}.

in agreement with those findings both in terms of rates (53 s^{-1} in the rapid phase reducing to a steady state of 10.5 s^{-1}) and amplitude of the rapid phase (~9 P_i per PcrA).

DISCUSSION

Characterization of Rhodamine-PBP. We have demonstrated that the specific labeling of a double cysteine mutant PBP by a rhodamine can produce a species whose fluorescence responds to P_i binding. The size of the fluorescence change depends on several factors. The first is the distance and accessibility between thiol-attached rhodamines and the movement during the P_i-associated conformation change. Examination of the crystal structures provided an initial assessment of this, taking into account the covalent structure of the labels to determine suitable distances that might allow

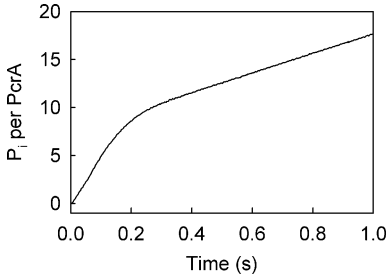

FIGURE 5: Use of rhodamine-PBP in a real-time assay of P_i production by the DNA helicase, PcrA. The reaction was carried out in a stopped-flow apparatus in a buffer of 50 mM Tris·HCl, 150 mM NaCl, and 3 mM $MgCl_2$ containing 10 μM rhodamine-PBP, 0.1 unit mL^{-1} PNPase, and 100 μM 7-methylguanosine. 50 nM PcrA and 1 μM dT_{20} were premixed so that essentially all PcrA is bound to the oligonucleotide, then rapidly mixed with 200 μM ATP. The fluorescence was followed with time. The signal was calibrated by consecutively introducing into the apparatus, 10 μM rhodamine-PBP alone, then the same solution containing either 0.5 μM P_i or 1 μM P_i. At each stage, the fluorescence was measured. All concentrations are those in the mixing chamber.

rhodamine−rhodamine interaction. Secondary effects, such as possible flexibility on the protein or interaction with amino acid side chains, are also likely to be important to give optimal orientations.

Another factor determining the fluorescence signal is optimal labeling. As described in the Results section, it is likely that only the double-labeled species can give the desired fluorescence response to P_i binding. A further factor is the ability to separate out other labeled species that are likely to have high fluorescence. The protocol described typically gives a product with ~18-fold fluorescence change. The best batch of product gave 30-fold, presumably due to the almost complete elimination of high fluorescence impurities. The variability of the fluorescence response between preparations (by ~2-fold) correlates approximately with the observed high fluorescence impurities shown by hplc. The main impurity is singly labeled PBP, which is typically <5% of total protein. This contaminant has the effect of increasing the fluorescence in the absence of P_i, and so reducing the ratio of fluorescence with and without P_i.

When the labeling sites are on the face of the molecule opposite from the binding cleft, the P_i site is unmodified. As described above, the surfaces of the two domains on this rear face move apart when P_i binds to its site, so the α-carbons of the two cysteines get separated further. This side of the protein is relatively open, so this distance change might be expected to be the main factor in determining a change in rhodamine stacking. With one such labeled mutant (K229C-E302C), a 10-fold increase in rhodamine fluorescence occurs on P_i binding, when the α-carbons move from 1.2 to 1.7 nm apart as determined from the crystal structures. However, in general these mutant proteins were variable in the degree of labeling and the final purity of the labeled protein. The K229C-E302C protein may be useful for further study, particularly where extra mutations to the binding site and cleft are required. In this case, both labeling sites are well away from the binding site and so may be neither affected by nor affect the binding of P_i.

A17C-A197C labeled with 6-IATR was the most satisfactory out of the several combinations of mutant proteins, as listed in Table 1, and rhodamine labels. This mutant, labeled with 6-IATR, gave up to 30-fold increase in fluorescence.

The α-carbons of these two amino acids are 1.6 and 1.3 nm apart in P_i-free and P_i-bound conformations of PBP, respectively. This is due to the binding cleft closure with each mutation being on opposite sides of the cleft. The absorbance spectra of purified rhodamine-PBP (Figure 1) suggest that there is almost complete dimer formation in the absence of P_i, and this ensures that the fluorescence is very low. The large increase in fluorescence suggests that there is a significant change in rhodamine−rhodamine interaction on P_i binding. Although the α-carbons get closer on P_i binding, the 197 position becomes partly buried, presumably constraining its attached rhodamine so that it can no longer interact well with the A17C rhodamine.

Rhodamine Stacking. The situation of two rhodamines being attached close to one another on a protein scaffold differs significantly from that of rhodamines that come into proximity either through high concentration in solution (*22*, *23*, *27*) or when both are attached to an unstructured peptide (*24*−*26*). In those situations, the two rhodamines associate by van der Waals interaction and take up relative positions that are unaffected by external constraints. The normal arrangement is a face-to-face stacking of the xanthene rings, but with a sideways displacement of the two ring systems relative to each other (*25*). The same arrangement is present in the solid state for rhodamine unattached to another molecule (*41*). In rhodamine-PBP, the two dyes remain close together whether or not P_i is bound and so it is likely that the dyes can interact in some way in both states, but the conformation change of the protein upon P_i binding alters the geometry of interaction. The relative orientation of the rhodamine dipoles in our examples is much less predictable, and a change of this orientation may contribute significantly to the change in fluorescence. The absorbance spectrum of the P_i-bound form differs from that of a simple monomeric rhodamine and supports the idea that interaction between monomers occurs in both conformations. We hope to obtain further optical and structural information on this in the course of future work.

Cysteine Thiol Accessibility. The reactions of DTNB with the double cysteine mutant and the two related single mutants show that there are minor effects on the reactivity of A17C depending on the presence of P_i or the other mutation. There is a much larger reduction of A197C reactivity due to the presence of P_i, compared to the reaction in the presence of the phosphate mop to minimize any phosphate. We suggested previously that the closed conformation may be nonreactive (*10*), so any reaction of A197C in the P_i-bound state may be due to a small amount of open conformation. This in turn may be due to the equilibrium proportion of open, but P_i-bound, conformation: this equilibrium is represented by step 2 of eq 1. These data support the idea that the A197C sulfur is partly buried when the conformation is closed, as suggested by the crystal structures. This means that it is important to use the phosphate mop when labeling, to ensure almost all protein is in the P_i-free, open conformation.

Properties of Rhodamine-PBP. The rhodamine in the labeled protein has different absorbance properties from that in free solution, so titrations with P_i were used to calculate an extinction coefficient (108 mM^{-1} cm^{-1}) for the labeled protein at its isosbestic point (526 nm). These data suggest that each rhodamine attached to the apoprotein has an absorbance at 528 nm, which is 14% less than that for a free rhodamine.

An important practical measure of the effectiveness of such a sensor is a titration of the labeled protein with P_i, as in Figure 3. This shows that the fluorescence response is linear over most of the titration, and it is likely that essentially all sites of the PBP can be bound similarly with P_i. In contrast, MDCC-PBP has an effective capacity of ∼70%. The likely explanation for this difference is the presence of diastereoisomers of MDCC-PBP as the linkage is via a chiral center on a succinimide (*10*, *11*). The diastereoisomers evidently have different fluorescence responses to P_i binding, giving rise to an apparently reduced activity. Here the rhodamine linkage via an iodoacetamide does not give rise to a new chiral center on reaction with a cysteine.

The kinetic data show that the association kinetics with this rhodamine-PBP (at 10 °C) are slightly slower than those found with MDCC-PBP at 5 °C. This may relate to the fact that the rhodamine interaction must be disrupted, providing a small additional barrier for cleft closure to occur. The overall dissociation constant (eq 1) is 70 nM. Thus, the tightness of binding is similar to that obtained with MDCC-PBP.

The MDCC-PBP sensor has found wide application for kinetic measurements in bulk solution, such as in stopped-flow measurements. We have now demonstrated that rhodamine-PBP can be used to measure rapid P_i formation in real time with results comparable to those described for a previously characterized reaction (*40*).

This new sensor has various differences from the coumarin-labeled PBP that suggest advantages and possibilities of wider application. Rhodamine is generally much more photostable than the MDCC coumarin. This confers an advantage where high-intensity illumination is required for extended time, for example, in single molecule studies or high throughput screening. The higher excitation wavelength of rhodamine may also be advantageous through a reduction in cellular autofluorescence. In the case of the K229C-E302C protein, the rhodamines of the new biosensor are distal to the P_i binding site and should not offer any interference with P_i binding. In contrast, MDCC-PBP has a fluorescence change that depends on precise interaction of the coumarin with the protein surface at the entrance of the binding site (*11*). In general, the double labeling strategy suggests that the rhodamine interaction (and hence fluorescence) should depend mainly on the distance and structural changes in the region of the labels. These should not be affected by changes in the P_i binding site. Precise understanding of the interactions between rhodamines will be enhanced by structural studies, but the changes in rhodamine stacking provide a novel probe for P_i that is both sensitive and robust.

ACKNOWLEDGMENT

We thank Dr. R. Munasinghe (NIMR, London) for technical assistance with preparation of 6-iodoacetamidotetramethylrhodamine and Dr. S. Howell (NIMR, London) for producing mass spectra.

REFERENCES

1. Webb, M. R. (2003) A fluorescent sensor to assay inorganic phosphate, in *Kinetic Analysis: A Practical Approach* (Johnson, K. A., Ed.) pp 131−152, Oxford University Press: Oxford, U.K.

2. Brune, M., Hunter, J. L., Corrie, J. E. T., and Webb, M. R. (1994) Direct, real-time measurement of rapid inorganic phosphate release using a novel fluorescent probe and its application to actomyosin subfragment 1 ATPase, *Biochemistry 33*, 8262−8271.
3. Lundgren, J. S., Salins, L. E., Kaneva, I., and Daunert, S. (1999) A dynamical investigation of acrylodan-labeled mutant phosphate binding protein, *Anal. Chem. 71*, 589−595.
4. De Lorimier, R. M., Smith, J. J., Dwyer, M. A., Looger, L. L., Sali, K. M., Paavola, C. D., Rizk, S. S., Sadigov, S., Conrad, D. W., Loew, L., and Hellinga, H. W. (2002) Construction of a fluorescent biosensor family, *Protein Sci. 11*, 2655−2675.
5. Tolosa, L., Gryczynski, I., Eichhorn, L. R., Dattelbaum, J. D., Castellano, F. N., Rao, G., and Lakowicz, J. R. (1999) Glucose sensor for low-cost lifetime-based sensing using a genetically engineered protein, *Anal. Biochem. 267*, 114−120.
6. Dattelbaum, J. D., and Lakowicz, J. R. (2001) Optical determination of glutamine using a genetically engineered protein, *Anal. Biochem. 291*, 89−95.
7. Gilardi, G., Zhou, L. Q., Hibbert, L., and Cass, A. E. G. (1994) Engineering the maltose binding protein for reagentless fluorescence sensing, *Anal. Chem. 66*, 3840−3847.
8. Gilardi, G., Mei, G., Rosato, N., Agro, A. F., and Cass, A. E. G. (1997) Spectroscopic properties of an engineered maltose binding protein, *Protein Eng. 10*, 479−486.
9. Luecke, H., and Quiocho, F. A. (1990) High specificity of a phosphate transport protein determined by hydrogen bonds, *Nature 347*, 402−406.
10. Brune, M., Hunter, J. L., Howell, S. A., Martin, S. R., Hazlett, T. L., Corrie, J. E. T., and Webb, M. R. (1998) Mechanism of inorganic phosphate interaction with phosphate binding protein from *Escherichia coli*, *Biochemistry 37*, 10370−10380.
11. Hirshberg, M., Henrick, K., Haire, L. L., Vasisht, N., Brune, M., Corrie, J. E. T., and Webb, M. R. (1998) The crystal structure of phosphate binding protein labeled with a coumarin fluorophore, a probe for inorganic phosphate, *Biochemistry 37*, 10381−10385.
12. Dattelbaum, J. D., Looger, L. L., Benson, D. E., Sali, K. M., Thompson, R. B., and Hellinga, H. W. (2005) Analysis of allosteric signal transduction mechanisms in an engineered fluorescent maltose biosensor, *Protein Sci. 14*, 284−291.
13. Hall, J. A., Thorgeirsson, T. E., Liu, J., Shin, Y., and Nikaido, H. (1997) Two modes of ligand binding in maltose-binding protein of *Escherichia coli*. Electron paramagnetic resonance study of ligand-induced global conformational changes by site-directed spin labeling, *J. Biol. Chem. 272*, 17610−17614.
14. White, H. D., Belknap, B., and Webb, M. R. (1997) Kinetics of nucleoside triphosphate cleavage and phosphate release steps by associated rabbit skeletal actomyosin, measured using a novel fluorescent probe for phosphate, *Biochemistry 36*, 11828−11836.
15. Bertram, J. G., Bloom, L. B., Hingorani, M. M., Beechem, J. M., O'Donnell, M., and Goodman, M. F. (2000) Molecular mechanism and energetics of clamp assembly in *Escherichia coli*. The role of ATP hydrolysis when γ complex loads β on DNA, *J. Biol. Chem. 275*, 28413−28420.
16. Gilbert, S. P., Webb, M. R., Brune, M., and Johnson, K. A. (1995) Pathway of processive ATP hydrolysis by kinesin, *Nature 373*, 671−676.
17. Nixon, A. E., Brune, M., Lowe, P. N., and Webb, M. R. (1995) Kinetics of inorganic phosphate release during the interaction of p21ras with the GTPase activating proteins, p120-GAP and neurofibromin, *Biochemistry 34*, 15592−15598.
18. He, Z.-H., Chillingworth, R. K., Brune, M., Corrie, J. E. T., Trentham, D. R., Webb, M. R., and Ferenczi, M. A. (1997) ATPase kinetics on activation of rabbit and frog permeabilized isometric muscle fibres: a real time phosphate assay, *J. Physiol. 501*, 125−148.
19. Kasha, M. (1963) Energy transfer mechanisms and the molecular exciton model for molecular aggregates, *Radiat. Res. 20*, 55−70.
20. Kasha, M., Rawls, H. R., and Ashraf El-Bayoumi, M. (1965) The exciton model in molecular spectroscopy, *Pure Appl. Chem. 11*, 371−392.
21. Scholes, G. D., and Ghiggino, K. P. (1994) Electronic interactions and interchromophore electron transfer, *J. Phys. Chem. 98*, 4580−4590.
22. Förster, T., and König, E. (1957) Absorptionsspektren und Fluoreszenzeigenschaften konzentrierter Lösungen organischer Farbstoffe, *Z. Elektrochem. 61*, 344−348.
23. Selwyn, J. E., and Steinfeld, J. I. (1972) Aggregation equilibria of xanthene dyes, *J. Phys. Chem. 76*, 762−774.
24. Geoghegan, K. F., Rosner, P. J., and Hoth, L. R. (2000) Dye-pair reporter systems for protein-peptide molecular interactions, *Bioconjugate Chem. 11*, 71−77.
25. Blackman, M. J., Corrie, J. E. T., Croney, J. C., Kelly, G., Eccleston, J. F., and Jameson, D. M. (2002) Structural and biochemical characterization of a fluorogenic rhodamine-labeled malarial protease substrate, *Biochemistry 41*, 12244−12252.
26. Packard, B. Z., Toptygin, D. D., Komoriya, A., and Brand, L. (1996) Profluorescent protease substrates: intramolecular dimers described by the exciton model, *Proc. Natl. Acad. Sci. U.S.A. 93*, 11640−11645.
27. Chambers, R. W., Kajiwara, T., and Kearns, D. R. (1974) Effect of dimer formation on the electronic absorption and emission spectra of ionic dyes, *J. Phys. Chem. 78*, 380−387.
28. Dietrich, A., Buschmann, V., Muller, C., and Sauer, M. (2002) Fluorescence resonance energy transfer (FRET) and competing processes in donor-acceptor substituted DNA strands: a comparative study of ensemble and single-molecule data, *Rev. Mol. Biotechnol. 82*, 211−231.
29. Bernacchi, S., and Mely, Y. (2001) Exciton interaction in molecular beacons: a sensitive sensor for short range modifications of the nucleic acid structure, *Nucleic Acids Res. 29*, e62.
30. Hamman, B. D., Oleinikov, A. V., Jokhadze, G. G., Bochkariov, D. E., Traut, R. R., and Jameson, D. M. (1996) Tetramethylrhodamine dimer formation as a spectroscopic probe of the conformation of *Escherichia coli* ribosomal protein L7/L12 dimers, *J. Biol. Chem. 271*, 7568−7573.
31. Nixon, A. E., Hunter, J. L., Bonifacio, G., Eccleston, J. F., and Webb, M. R. (1998) Purine nucleoside phosphorylase: its use in a spectroscopic assay for inorganic phosphate and to remove inorganic phosphate with the aid of phosphodeoxyribomutase, *Anal. Biochem. 265*, 299−307.
32. Bird, L. E., Brannigan, J. A., Subramanya, H. S., and Wigley, D. B. (1998) Characterisation of *Bacillus stearothermophilus* PcrA helicase: evidence against an active rolling mechanism, *Nucleic Acids Res. 26*, 2686−2693.
33. Corrie, J. E. T., and Craik, J. S. (1994) Synthesis and characterisation of pure isomers of iodoacetamidotetramethylrhodamine, *J. Chem. Soc. Perkin Trans. I*, 2967−2974.
34. Munasinghe, V. R. N., and Corrie, J. E. T. (2006) Optimised synthesis of 6-iodoacetamidotetramethylrhodamine, *ARKIVOC ii*, 143−149.
35. Leatherbarrow, R. J. (2001) *Grafit Version* 5, Erithacus Software Ltd., Horley, U.K.
36. Ledvina, P. S., Yao, N., Choudhary, A., and Quiocho, F. A. (1996) Negative electrostatic surface potential of protein sites specific for anionic ligands, *Proc. Natl. Acad. Sci. U.S.A. 93*, 6786−6791.
37. Clearfield, A., and Duax, W. L. (1969) The crystal structure of the ion exchanger zirconium bis(monohydrogen orthoarsenate) monohydrate, *Acta Crystallogr. B25*, 2658−2662.
38. Byers, L. D., She, H. S., and Alayoff, A. (1979) Interaction of phosphate analogs with glyceraldehyde-3-phosphate dehydrogenase, *Biochemistry 18*, 2471−2480.
39. Ali, B. R. S., and Dixon, H. B. F. (1992) Pyridoxal arsenate as a prosthetic group for aspartate aminotransferase, *Biochem. J. 284*, 349−352.
40. Dillingham, M. S., Wigley, D. B., and Webb, M. R. (2000) Demonstration of unidirectional single-stranded DNA translocation by pcrA helicase: measurement of step size and translocation speed, *Biochemistry 39*, 205−212.
41. Cavallo, L., Moore, M. H., Corrie, J. E. T., and Fraternali, F. (2004) Quantum mechanics calculations on rhodamine dyes require inclusion of solvent water for accurate representation of the structure, *J. Phys. Chem. A 108*, 7744−7751.

BI060960J